Supplementary Information

Bidirectional Manipulation of Iodine Redox Kinetics in Aqueous Fe-I_2 Electrochemistry

Weiwei Zhang[a,b,1], Mingli Wang[a,c,1], Hong Zhang[d,*], Lin Fu[e], Wenli Zhang[f], Yupeng Yuan[a,*], and Ke Lu[a,c,*]

[a]Institutes of Physical Science and Information Technology, School of Materials Science and Engineering, Key Laboratory of Structure and Functional Regulation of Hybrid Materials of Ministry of Education, Anhui University, Hefei, Anhui 230601, China.
[b]School of Chemistry and Chemical Engineering, Qufu Normal University, Qufu, Shandong 273165, China.
[c]Hefei National Laboratory for Physical Sciences at the Microscale, Hefei, Anhui 230026, China.
[d]School of Chemistry and Chemical Engineering, Harbin Institute of Technology, Harbin, Heilongjiang 150001, China.
[e]School of Chemistry and Chemical Engineering, Guizhou University, Guiyang, Guizhou 550025, China.
[f]School of Chemical Engineering and Light Industry, Guangdong University of Technology, Guangzhou, Guangdong 510006, China.
[1]W.Z. and M.W. contributed equally to this work.

*Correspondence: zhanghonghit@hit.edu.cn (H.Z.); yupengyuan@ahu.edu.cn (Y.Y.); luke@ahu.edu.cn (K.L.)

Sample preparation

In a typical process, 1.5 mL aniline monomer was added into 30 mL phytic acid (PA) solution. The wiper cloth was and immersed in the above solution under stirring, and the mixture was cooled to ~4 ℃ via the ice bath. Subsequently, the 20 mL aqueous solution containing the 1.8 g of $FeCl_3$ was slowly added into the mixture to initiate the chemical oxidative polymerization of aniline, resulting in the Fe^{n+}-doped polyaniline -phytic acid (PANi-PA) shell that interfacial wrapped on the wiper cloth fiber surface. The resultant cloth was washed with a large amount of distilled water and dried at 60 ℃, followed by annealing at 900 ℃ for 1 h with the presence of NaH_2PO_2 as the phosphorus source. During this procedure, the Fe-doped PANi-PA shell was carbonized into nitrogen and phosphorus co-doped carbon shell with uniformly decorated FeP nanoparticles. The obtained sample was named FeP-NPC-CC. For comparison, the control sample of NPC-CC was prepared as the identical process that just replace the $FeCl_3$ with ammonium persulfate. The CC baseline sample was directly realized by annealing the wiper cloth at 900 ℃. For the preparation of iodine cathodes, enough iodine was put in DI water to measure the iodine number. According to the increasing mass of carbon cloth before and after adsorption, the iodine mass loading can be obtained. The prepared iodine cathodes were dried at 80 °C to remove water.

Sample characterization

The phase purity and crystal structure of the samples were determined by the X-ray diffraction patterns using a Rigaku Miniflex diffractometer (Rigaku Corporation, Japan). X-ray photoelectron spectroscopy was performed using an ESCALAB 250 X-ray photoelectron spectrometer. The Brunauere-Emmete-Teller (BET)-specific surface area was determined by nitrogen adsorption-desorption measurements conducted at 77 K using the TriStar 3000 analyzer. Pore size distribution curves were computed from the desorption branches of the isotherms using the Barrett, Joyner, and Halenda (BJH) method. The Raman spectra were collected by the LabRAM HR 800 system with a 532 nm excitation laser. UV-Vis measurement was conducted using a Shimadzu UV-1800 spectrophotometer. Structural and morphological characterization of the samples was conducted using scanning electron microscopy (Hitachi 650 electron microscope) and transmission electron microscopy (JEM-2100F microscope with a Bruker EDS detector). The iodine loading content and thermostability of the iodine-carbon composite was determined by thermogravimetric analysis under an N_2 atmosphere in the TG/DTA6300 analyzer, from room temperature to 500 °C with a ramp rate of 10 °C min^{-1}.

Electrochemical measurements

The free-standing cathodes were cut into discs of 1.2 cm and directly used as the working electrodes with the iodine mass loading in the range of 1.5-2.6 mg cm^{-2}. The baseline electrodes for testing were prepared via the same procedure. The Fe foil (99.99%) and Fe powder were modified with ascorbic acid (0.2 M) for 12 h before used as anode. Electrochemical tests for Fe-I_2 cells were performed using CR2016-type coin cells, employing the Fe foil as the anode and 1 M $FeSO_4$ as the electrolyte. Glass fiber paper was employed as separator. All cycle volt measurements (CV) were performed with a CHI 760e electrochemical workstation. The galvanostatic charged and discharged tests of Fe-I_2 cells were recorded on the battery testing system (Neware BTS-4000 battery analyzer) with a potential window of 0.4-12 V at room temperature. Capacities are calculated based on the mass of iodine.

Beaker cell assemble and measurement

The beaker cell was employed for the visual experiments, where the 4 mL of the standard electrolyte was used for sufficiently immersing I_2/FeP-NPC-CC, I_2/NPC-CC, and I_2/CC electrodes and Fe foils. The iodine loading for all positive electrodes was 2 mg cm^{-1} and the active area (immersion area) was about 1 cm^2. After 100 cycles charge/discharge, the absorption ability of different substrates towards active iodine was compared by the color change of the electrolyte.

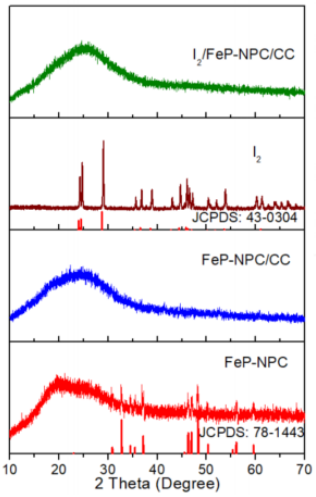

Figure S1. XRD patters of as-prepared samples.

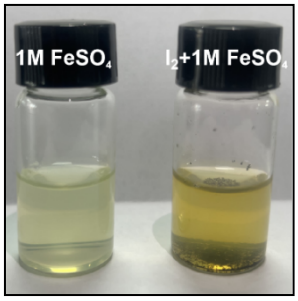

Figure S2. Photographs of the 1M $FeSO_4$ solution (left) and I_2+1M $FeSO_4$ solution (right).
It can be observed that the color of the solution transforms from light green to a yellowish color when iodine is added, which can be used as direct visual evidence to determine the migration of iodine species into the solution.

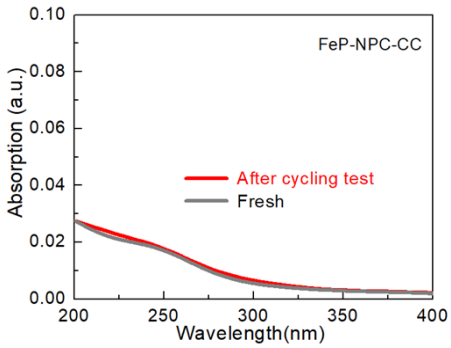

Figure S3. UV-Visible absorption spectra of the electrolyte of the Fe//FeP-NPC-CC cell before and after the cycling stability test.
As shown, there is no obvious change of the electrolyte of the cycled Fe//FeP-NPC-CC cell. This result confirms the high stability of the composite matrix and the color change in Figure 3d attributed to the I_2 or polyiodide species rather than the dissolved iron ions.

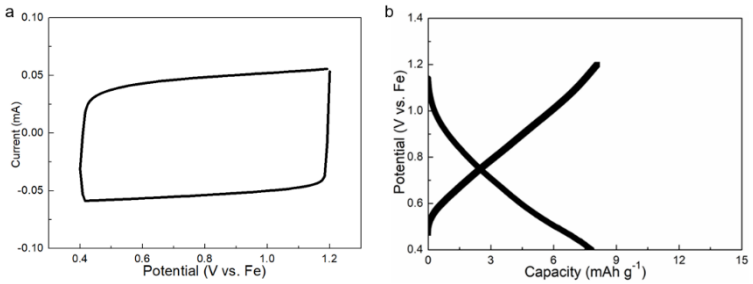

Figure S4. (a) Cyclic voltammogram (at 0.1 mV s^{-1}) and (b) galvanostatic charge-discharge profiles of FeP-NPC-CC composite without iodine.

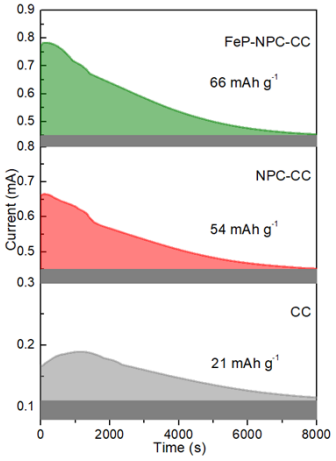

Figure S5. Potentiostatic discharge curves of I_2 solution at 0.75 V on the surfaces of FeP-NPC-CC, NPC-CC and CC supports.

Table S1. Comparison of the iodine content and electrochemical performance for the I_2/FeP-NPC-CC cathodes and other reported works.

Cathode	Iodine loading (%)	Capacity (mAh g_{iodine}^{-1})	Ref.
I_2/FeP-NPC-CC	**52**	**202**	**This work**
I_2/N-HPC	40	190	[1]
N-LPC/I_2	44	137	[2]
I-BC_{HP}	41	115	[3]
MPC/I_2	41	120	[4]
I_2@KB	50	200	[5]
ZPC/I_2	22	198	[6]
I_2/OSTC	26.6	185	[7]
I_2/ACF	40	160	[8]

Table S2. Comparison of electrochemical performance for Fe-I_2 cell with state-of-the-art reported aqueous multivalent ion batteries.

Cathode	Anode type (Cation)	Discharge capacity (mAh g^{-1})	Cycling stability	Ref.
I_2/FeP-NPC-CC	**Fe (Fe^{2+})**	**202/0.2 Ag^{-1}**	**92%/500 cycles/0.5 Ag^{-1}**	**This work**
$Fe[Fe(CN)_6]_{0.75\cdot\square 0.25\cdot 3.5}H_2O$	Fe (Fe^{2+})	58/2 C	80%/1000/10 C	[9]
$VOPO_4{\cdot}2H_2O$	Fe (Fe^{2+})	100/0.1 Ag^{-1}	62.5%/800/0.8 Ag^{-1}	[10]
I_2/CC	Zn (Zn^{2+})	335/1 mA cm^{-1}	91%/200 cycles/2 mA cm^{-2}	[11]
NSGF	Zn-NSGF (Zn^{2+})	88/0.1 Ag^{-1}	79%/300 cycles/0.2 Ag^{-1}	[12]
$[ZnI_x(OH_2)_{4-x}]^{2-x}$	Zn (Zn^{2+})	-	80%/500/0.3 mA cm^{-2}	[13]
I_2/C	Zn (Zn^{2+})	219/0.5 C	62%/1000/1 C	[14]
N-LPC/I_2	Zn (Zn^{2+})	127/0.1 Ag^{-1}	96%/100/0.1 Ag^{-1}	[1]
I_2-BC_{HP}	Zn (Zn^{2+})	115/0.1 Ag^{-1}	80%/150/0.1 Ag^{-1}	[2]
CF/I_2	Zn (Zn^{2+})	110/0.1 Ag^{-1}	70%/300/0.1 Ag^{-1}	[3]
ZnHCF@MnO_2	Zn (Zn^{2+})	118/0.1 Ag^{-1}	77/1000/0.5 Ag^{-1}	[15]
MnPBA HSs	Zn (Zn^{2+})	85.9/0.05 Ag^{-1}	53.6%/1000/1 Ag^{-1}	[16]
CuHCF	MoO_3@PPy (Al^{3+})	31/0.2 Ag^{-1}	83.2%/100/0.2 Ag^{-1}	[17]
Mg-OMS-1	$FeVO_4$/C (Mg^{2+})	58.9/0.1 Ag^{-1}	97.7%/100/0.05 Ag^{-1}	[18]
ZnHCF	ITO (Ca^{2+})	75.3/0.4 Ag^{-1}	-	[19]

Reference

[1] Y. Ji, J.W. Xu, Z.R. Wang, M.M. Ren, Y. Wu, W.L. Liu, J.S. Yao, C.B. Zhang, H. Zhao, Nitrogen-doped litchi-shell derived porous carbon as an efficient iodine host for zinc-iodine batteries, J. Electroanal. Chem. 931 (2023) 8.

[2] J.W. Xu, W.Q. Ma, L.H. Ge, M.M. Ren, X.X. Cai, W.L. Liu, J.S. Yao, C.B. Zhang, H. Zhao, Confining iodine into a biomass-derived hierarchically porous carbon as cathode material for high performance zinc-iodine battery, J. Alloy. Compd. 912 (2022) 8.

[3] Y.Z. Hou, F.G. Kong, Z.R. Wang, M.M. Ren, C.D. Qiao, W.L. Liu, J.S. Yao, C.B. Zhang, H. Zhao, High performance rechargeable aqueous zinc-iodine batteries via a double iodine species fixation strategy with mesoporous carbon and modified separator, J. Colloid Interface Sci. 629 (2023) 279-287.

[4] C. Bai, H.J. Jin, Z.S. Gong, X.Z. Liu, Z.H. Yuan, A high-power aqueous rechargeable Fe-I₂ battery, Energy Storage Mater. 28 (2020) 247-254.

[5] Z. Cheng, H. Pan, F. Li, C. Duan, H. Liu, H.Y. Zhong, C.C. Sheng, G.J. Hou, P. He, H.S. Zhou, Achieving long cycle life for all-solid-state rechargeable Li-I₂ battery by a confined dissolution strategy, Nat. Commun. 13(1) (2022) 9.

[6] J.W. Xu, J.G. Wang, L.H. Ge, J.R. Sun, W.Q. Ma, M.M. Ren, X.X. Cai, W.L. Liu, J.S. Yao, ZIF-8 derived porous carbon to mitigate shuttle effect for high performance aqueous zinc-iodine batteries, J. Colloid Interface Sci. 610 (2022) 98-105.

[7] M.Y. Chen, W.X. Zhu, H.L. Guo, Z.H. Tian, L.Q. Zhang, J.T. Wang, T.X. Liu, F.L. Lai, J.J. Huang, Tightly confined iodine in surface-oxidized carbon matrix toward dual-mechanism zinc-iodine batteries, Energy Storage Mater. 59 (2023) 8.

[8] H.L. Pan, B. Li, D.H. Mei, Z.M. Nie, Y.Y. Shao, G.S. Li, X.H.S. Li, K.S. Han, K.T. Mueller, V. Sprenkle, J. Liu, Controlling Solid-Liquid Conversion Reactions for a Highly Reversible Aqueous Zinc-Iodine Battery, ACS Energy Lett. 2(12) (2017) 2674-2680.

[9] X.Y. Wu, A. Markir, Y.K. Xu, C. Zhang, D.P. Leonard, W. Shin, X.L. Ji, A Rechargeable Battery with an Iron Metal Anode, Adv. Funct. Mater. 29(20) (2019) 7.

[10] Y.K. Xu, X.Y. Wu, S.K. Sandstrom, J.J. Hong, H. Jiang, X. Chen, X.L. Ji, Fe-Ion Bolted VOPO₄•2H₂O as an Aqueous Fe-Ion Battery Electrode, Adv. Mater. 33(49) (2021) 7.

[11] Y.X. Li, L.J. Liu, H.X. Li, F.Y. Cheng, J. Chen, Rechargeable aqueous zinc-iodine batteries: pore confining mechanism and flexible device application, Chem. Commun. 54(50) (2018) 6792-6795.

[12] K. Lu, H. Zhang, B. Song, W. Pan, H.Y. Ma, J.T. Zhang, Sulfur and nitrogen enriched graphene foam scaffolds for aqueous rechargeable zinc-iodine battery, Electrochim. Acta 296 (2019) 755-761.

[13] J.J. Hong, L.D. Zhu, C. Chen, L.T. Tang, H. Jiang, B. Jin, T.C. Gallagher, Q.B. Guo, C. Fang, X.L. Ji, A Dual Plating Battery with the Iodine/ ZnI_x(OH₂)_{4-x} ^{2-x} Cathode, Angew. Chem.-Int. Edit. 58(44) (2019) 15910-15915.

[14] Z.P. Huang, W.W. Zhang, H. Zhang, L. Fu, B. Song, W.L. Zhang, Q.W. Chen, K. Lu, Uniform zinc electrodeposition directed by interfacial cation reservoir for stable Zn-I₂ battery, J. Power Sources 523 (2022) 7.

[15] K. Lu, B. Song, Y.X. Zhang, H.Y. Ma, J.T. Zhang, Encapsulation of zinc hexacyanoferrate nanocubes with manganese oxide nanosheets for high-performance rechargeable zinc ion batteries, J. Mater. Chem. A 5(45) (2017) 23628-23633.

[16] Y.X. Zeng, X.F. Lu, S.L. Zhang, D.Y. Luan, S. Li, X.W. Lou, Construction of Co-Mn Prussian Blue Analog Hollow Spheres for Efficient Aqueous Zn-ion Batteries, Angew. Chem.-Int. Edit. 60(41) (2021) 22189-22194.

[17] P.P. Wang, Z. Chen, Z.Y. Ji, Y.P. Feng, J.Q. Wang, J. Liu, M.M. Hu, H. Wang, W. Gan, Y. Huang, A flexible aqueous Al ion rechargeable full battery, Chem. Eng. J. 373 (2019) 580-586.
[18] H.Y. Zhang, K. Ye, K. Zhu, R.B. Cang, J. Yan, K. Cheng, G.L. Wang, D.X. Cao, High-Energy-Density Aqueous Magnesium-Ion Battery Based on a Carbon-Coated FeVO₄ Anode and a Mg-OMS-1 Cathode, Chem.-Eur. J. 23(67) (2017) 17118-17126.
[19] P.P. Wang, H. Wang, Z. Chen, J.W. Wu, J.T. Luo, Y. Huang, Flexible aqueous Ca-ion full battery with super-flat discharge voltage plateau, Nano Res. 15(1) (2022) 701-708.